BNL-211964-2019-TECH
CBETA/045

Hysteresis and degaussing of H1 dipole magnets

M. S. Fabus, S. Peggs

July 2019

Collider Accelerator Department
Brookhaven National Laboratory

U.S. Department of Energy
USDOE Office of Science (SC), Nuclear Physics (NP) (SC-26)

DISCLAIMER

Hysteresis and Degaussing of H1 Dipole Magnets

Marco S. Fabus

Department of Physics, University of Oxford, UK
CBETA, Cornell University / BNL, USA

July 30, 2019

Abstract

Hysteresis was observed in the H1 dipole magnets in CBETA SX line. This study is the first step in order to understand and mitigate the effects this has on field reproducibility. Ansys Maxwell 19.2 was used to model the MS1DIP05 magnet with a hysteretic core. The parameter space for a degaussing procedure using the trim coils was explored. It was found that significant degaussing can be obtained with a decaying ringing waveforms of magnitudes above 10 A, so long as the frequency f and decay constant w were chosen such that $f \gg w$. The circuit properties of the magnet were simulated and explored using a sinusoidal voltage input. It was found that for low frequencies $f \ll 1\,\mathrm{Hz}$, the magnet behaves as a series LR circuit with $R = (28.3 \pm 0.5)\,\mathrm{m\Omega}$ and $L = (5.7 \pm 0.1)\,\mathrm{mH}$. At higher frequencies, hysteretic effects become significant, and resistance becomes proportional to the frequency due to hysteretic losses. A drop and saturation in inductance for higher frequencies was observed in the simulation data. Numerical instabilities were found for excitations below small voltages $V < 50\,\mathrm{mV}$. Experimental results on degaussing and current corrections were collected with Hall probe measurements. Good qualitative agreement with simulation results was found, but due to B-H curve details quantitative comparisons were inaccurate. Two procedures, MaxOp and MaxNull, were designed to produce repeatable operating field values to within 0.1 G.

Keywords: MS1DIP05, Hysteresis, Degaussing, Ansys Maxwell, Reproducible Field Production

Acknowledgements

This work was done under the supervision and guidance of several CBETA team members, mainly Scott Berg, Dave Burke, Steve Peggs, and Jim Crittenden. Further help with geometric models and Ansys documentation was given by Myka Umali. Getting Ansys running was thanks to the great CLASSE IT team, especially Attilio De Falco. Support and encouragement in various forms was also given by other CLASSE REU 2019 students. Financially, this work was made possible by St. John's College, University of Oxford, and Brookhaven National Laboratory, USA.

This author would like to express their gratitude to all the above for a stimulating summer project and for strengthening the U.S./EU Accelerator Physics partnerships.

Contents

1 Introduction

Magnetic hysteresis first began to be described around the beginning of the 20th century. At first it was of little practical use, but soon became important to understand. Its presence cause many ships in WW2 to retain a remnant field aligned with that of Earth's magnetic field, allowing German naval mines to sink unsuspecting ships. The understanding of hysteresis and its removal became a matter of life and death. A procedure for removing the remnant field was found and named *degaussing*, after the unit Gauss, then commonly used mainly by the Germans. Here a massive coil was installed around the ship and large currents were pulsed through in alternating directions to remove magnetic memory. A sister procedure called *wiping* was also designed, where a large cable was dragged around the ship with a pulsing 2000 A current. This helped save many lives during the Dunkirk evacuation. Most of these techniques were pioneered by Charles F. Goodeve, a Canadian chemist in the British navy.

Hysteresis did not cause as many deaths in the following decades, but stayed important as technologies developed. It became a principal effect in magnetic tapes, CRT monitors, magnetic memory, and many accelerators. It is this last application which is of concern to us. A prototype state-of-the-art Energy Recovery Linac (ERL) accelerator - the Cornell-BNL ERL Test Accelerator (CBETA) - is being commissioned at Cornell in 2019. A unique feature of the machine is its single return arc, which transports beams with energies from 42 to 150 MeV, achieved in as many as 4 accelerating passes through a single superconducting RF cryomodule, with energy recovery performed in 4 subsequent decelerating passes. A key part of the machine are the Elytt dipole electromagnets, which form part of the splitter (SX) and recombiner (RX) lines (see Fig. 1). Hysteresis was observed in these, principally in the H1 short dipole magnet type. This has caused issues with reproducibility of the magnetic field, and brought about a need for an unnecessary current correcting procedure. It is desirable to model these hysteretic effects, understand their nature, and devise strategies for mitigating their effects. This was the subject of the following study.

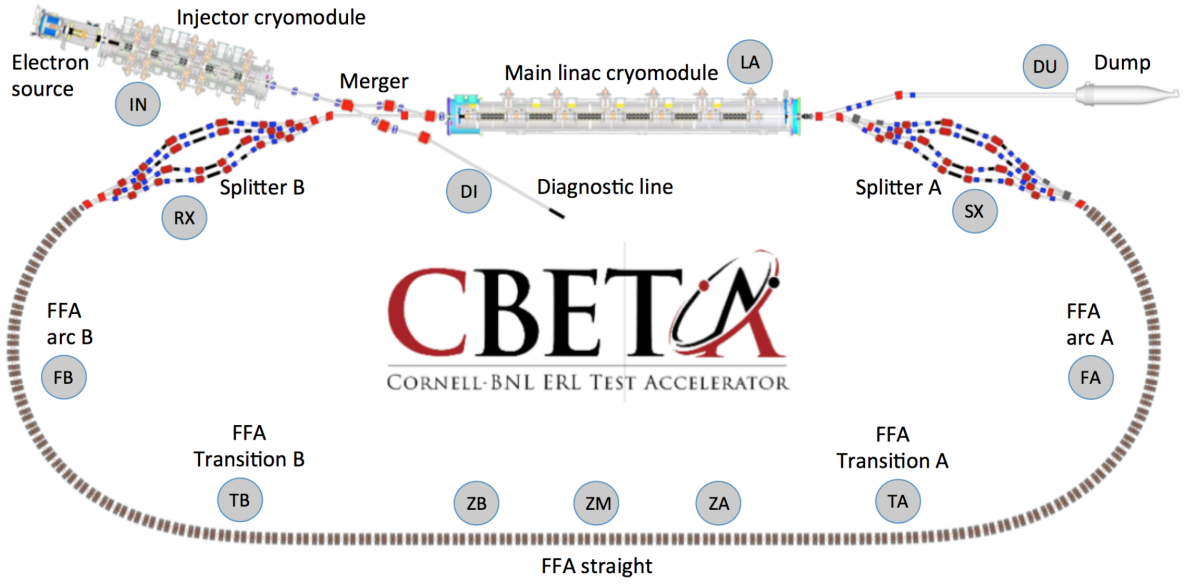

Figure 1: CBETA Machine Layout

The theory of hysteresis is first outlined, in a simplified yet sufficient form. Afterwards the Ansys Maxwell hysteresis simulations are explained and results given. Finally, first experimental results are established and future work suggested.

2 Theory

2.1 Introduction to Hysteresis Modelling

Hysteresis is one of the distinguishing features of ferromagnetic materials. It is a ubiquitous phenomenon in modern technology, ranging from magnetic memory to electric motors, transformers, and accelerator magnets. However, its essence is non-linear and history dependent, which makes it a complicated analytical and computational problem. It poses many challenges for an accurate and convergent description without unrealistic computation times or memory usage. In this section, we present a brief and simplified overview of the common approaches used, including that employed by our Maxwell Ansys 19.2 simulation software.

An important thing to note is that the treatment here is scalar, i.e. assuming isotropic hysteresis properties in the material. This assumption is not necessary in modern simulation packages (such as Ansys Maxwell), but it significantly simplifies the theoretical basis outlined below and is satisfactory for our case of simple low carbon steel used in the H1 yoke. For a more complete treatment, see [7].

2.1.1 Magnetisation Curves

Hysteresis in a ferromagnet is principally characterised by its hysteresis loop, i.e. a plot of the magnetisation as a function of applied magnetic field. However, a more common description is the $B - H$ curve, where the magnetic flux density B is assumed to have a dominant magnetisation contribution, as is the case for most ferromagnets. The main parameters defining a hysteresis curve are the remnant field (B at $H = 0$), coercive field (H at $B = 0$), and saturation flux density (B for the large H limit). For an example curve, see e.g. Fig. 2.

Most aspiring and practising physicists would have come across a simple hysteresis loop like the one mentioned above. However, this so-called saturation loop is only one from an infinite set of magnetisation curves. Anticipating later sections, here we are principally interested in the anhysteretic curve and the minor loops.

The *anhysteretic curve* is formed as a limiting case of return branches, like the ones seen in 2. These come in different orders, where the ones shown are progressively higher-order return branches. Choosing appropriate reversal fields allows us to jump between different return loops, and as such reach a state with no prior memory, i.e. the demagnetised state. Adding a small constant dc field atop this process moves us along the anhysteretic curve (from the Greek $\alpha\nu$-, indicating negation, and $\nu\sigma\tau\epsilon\rho o\zeta$, meaning "late"), as in Fig. 2. This is the basis for the process known as *degaussing*, i.e. removing a remnant magnetisation of a permanent magnet by applying a decaying oscillatory field to erase the memory of the system.

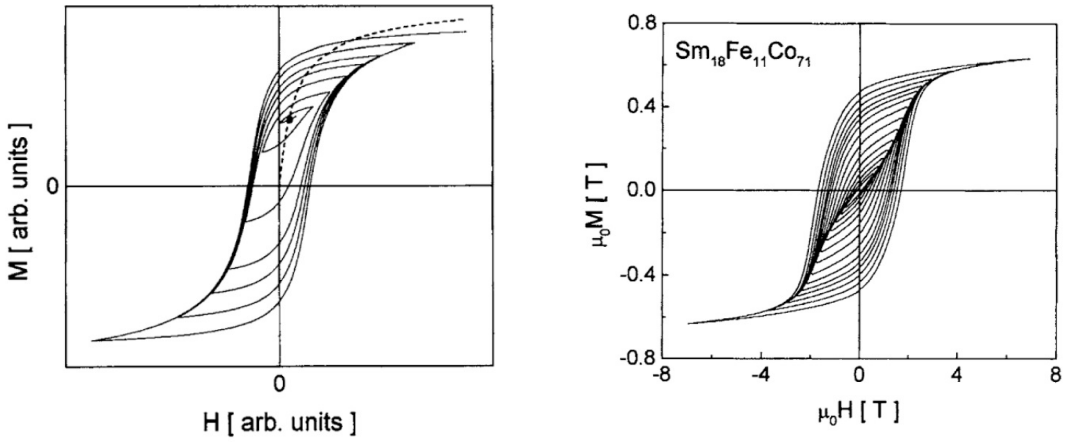

Figure 2: Example anhysteretic curve (left) and minor loops (right), from [7]

The *minor loops* are created when a cyclic field of variable amplitude is applied to the demagnetised state, as in Fig. 2. These are important as they contribute to circuit behaviour of electromagnets. A solenoid with a ferromagnetic core will exhibit higher resistance under an applied AC signal than that of the bare solenoid. This is due to *hysteresis loss*, a process where moving around the B-H curve dissipates energy proportional to that of its area. This result comes from the energy per unit volume injected into the magnetic specimen when completing a loop being

$$\oint_{loop} \vec{H} \cdot \mathrm{d}\vec{B}$$

(from Maxwell's equations). Thus knowledge of the minor loops is necessary to model circuit behaviour of hysteretic magnetic circuit elements.

2.1.2 Preisach Models

One of the oldest and best-established set of models that can reproduce this behaviour is that of Preisach. First described in Franz Preisach's 1935 paper, the fundamental building block of this model is a *Preisach hysteron*. This is a special hysteretic function defined as follows:

$$\gamma = \begin{cases} 0 & x < \alpha \\ \text{no change} & \alpha \leq x \leq \beta \\ 1 & x > \beta \end{cases}$$

This function is then given a hysteron density $p(x, y)$ in the *Preisach plane*, and normalised magnetisation can be found simply as

$$\iint \gamma p(x, y) \mathrm{d}x \mathrm{d}y.$$

This forms the basis of the Scalar Preisach Model, where in the simplest case hysteron density can be determined using an experimental saturation curve, and from this initial state minor loops and other quantities can be calculated. However, this model has significant shortcomings for our purposes. The main one is memory requirements, because history for each Preisach hysteron needs to be recorded and accessible. Another is hysteron independence, which means no anisotropy or

domain wall movement can be modelled. This can be addressed with more complicated versions of this basic model, but this is not the approach preferred by most modern simulation packages.

2.2 Ansys Maxwell Hysteresis Model

The simulation package of choice for CBETA transient simulations is Ansys Maxwell. This is part of an extremely powerful software package that forms the Ansys Workbench. With regards to hysteresis, Maxwell employs a variant of the Prandtl-Ishlinskii (PI) model, both of the play and stop type. In simplified terms, the field is decomposed into reversible and irreversible components, such that

$$\vec{H} = \vec{H}_{re} + \vec{H}_{ir},$$

with $\vec{B}$ then determined as

$$B = \mu_0 M(H_{re}) + \mu_0 H_{ir},$$

where vector signs were omitted as in our case the material is isotropic. Minor loops are formed from the recoil lines $B = \mu_0(H - H_c)$, where H_c is the coercivity. This assumed a constant slope between major branches, as is common for play and stop hysterons. See [6] for more technical details.

The PI model has major advantages compared to simpler Preisach models. For one, it is very user-friendly, because all Maxwell needs to determine minor loops and anhysteretic curves is one side of the saturated B-H loop, or even just the coercivity and remnant field in some cases. This makes it easy to work with whilst still faithfully representing hysteretic behaviour, including rotational losses (anisotropy). It is also less memory-intensive than basic Praisach models, as only $H_{re}(0)$ is required, i.e. the history of the reversible field need not be tracked (as it is linear by definition).

2.3 Back of the Envelope Calculations

2.3.1 Operating Fields and Degaussing Current Estimates

We can get order of magnitude estimates for quantities used later from simple electromagnetic arguments. Starting from Maxwell's equations in steady state,

$$\oint \vec{H} \cdot \mathrm{d}\vec{l} = I_{enc}.$$

Taking the material as linear for now with permeability μ, this means

$$NI = \int_{gap} \frac{\vec{B} \cdot \mathrm{d}\vec{l}}{\mu_{air}} + \int_{yoke} \frac{\vec{B} \cdot \mathrm{d}\vec{l}}{\mu_{Fe}}.$$

Assuming the window frame geometry of H1 as specified in [4], this evaluates to

$$NI = \frac{Bh}{\mu_{air}} + \frac{B\lambda}{\mu_{Fe}} \approx \frac{Bh}{\mu_0},$$

where h is the length of the air gap and λ effective length of magnetic flux lines in the yoke. Finally, this means

$$B = \frac{\mu_0}{h} NI \approx 0.7\,\mathrm{T}, \tag{1}$$

using $N = 52 \times 2, I = 187\,\text{A}, h = 3.6\,\text{cm}$, as specified in [4]. This is the operating field magnitude we should expect from our Maxwell simulation with a steady main coil current, and it compares well with 0.652 T in [1].

For the degaussing procedure, experimentally we know the remnant field to be about 15 G or 0.0015 T. From the above, we can estimate the necessary degaussing current as

$$I_d = \frac{Bh}{\mu_0 N} \approx 1.3\,\text{A},$$

with the trim coil of $N = 2 \times 17$ used. However, literature recommends (see e.g. [2]) a degaussing current of at least five times this value to have an appreciable effect, meaning we should expect significant degaussing with currents above $I_d = 6\,\text{A}$.

2.3.2 Gapped Solenoids as Circuit Elements

In subsequent sections we look at the simulated AC response of the H1 short dipole. We expect it to behave as an air-gapped solenoid, and hence can estimate the orders of magnitude of the inductance L and resistance R of the system. Main sources of resistance are the copper coil itself and hysteretic loss. Thus, at low frequencies, resistance should be close to the bare coil specified in [1], i.e. $0.03\,\Omega$. For higher frequencies hysteretic loss dominates and resistance becomes linear in frequency, since each pass around the hysteresis loop gives a fixed amount of loss.

The same document specifies the coil inductance in the gapped solenoid system as 4.5 mH, but we can get an order of magnitude estimate from energy considerations. Assuming iron to have infinite permeability, all the energy is stored in the gap, hence

$$E = \frac{1}{2} L I^2 = \frac{1}{2\mu_0} B^2 \times hA,$$

where I is the operating current, B the magnetic field, and hA the volume of the gap. From Eqn. 1 and rearranging,

$$L = \frac{\mu_0 N^2 A}{h} \approx 4\,\text{mH},$$

depending on the exact effective area used. This should be the inductance of the coil, at least if the system behaves as a simple R-L circuit.

3 Ansys Maxwell Simulations

The software used was Ansys EM Maxwell 3D 19.2, provided by Cornell University. In particular, the transient solver module was used throughout. This module solves Maxwell's equations using a finite element approach. Quantities solved for are the magnetic field $\vec{H}$ and the current density $\vec{J}$, from which other quantities, including the magnetic flux density $\vec{B}$, are automatically derived. This powerful module can consider arbitrary voltage oscillations, non-linear anisotropic permeabilities, and permanent magnets, amongst other things. More information can be found in [5].

3.1 General Setup and Verification

The geometric model used was provided by the CBETA team and prepared by Dave Burke. The particular magnet studied was the element MS1DIP05, also known as H1 Short Dipole. Its geometry and position in the beamline are in Fig. 3. Meshing was done in Maxwell, with mesh elements of average RMS length of about 25mm. Full mesh statistics are in the Appendix Tab. 7.3. This rather coarse mesh was chosen due to computational limitations, as hysteretic simulations are intense on resources, and at the time of this project full parallelisation of Maxwell tasks had not been set up on the Compute Farm.

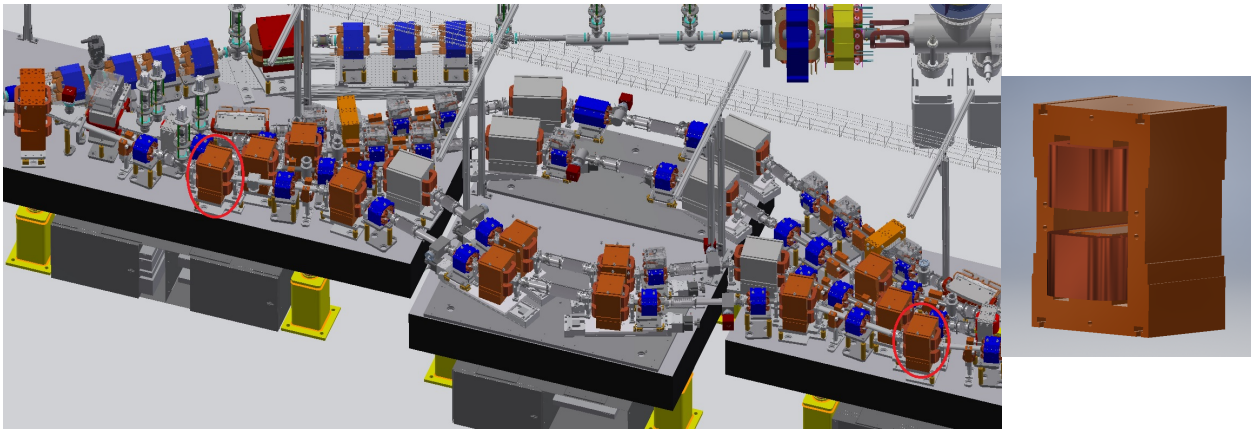

Figure 3: Position of the H1 studied in the SX line (left, circled) and the full geometry of the model (right)

Materials needed to be assigned after setting up the geometry and mesh. The coils were taken to be the default Maxwell copper material. The yoke was taken to be made of low-carbon steel, known as ALLIEDPUREIRON from our HMK Stahl provider. Iron with $\mu_r = 4000$ was used for linear simulations. The hysteretic magnetic properties used are specified in Fig. 4. These match the manufacturer reference sheets (see [4]), but use the higher H_c estimate. This is because in an initial phenomenological study, magnets were experimentally observed to posses hysteresis on order of 15 G or 1.5 mT, which suggested a higher coercivity value of around 140 Am^{-1}. This in turn suggested the carbon content in the magnet studied is on the higher end of specification values, as e.g. Fig. 4 suggests.

After successfully setting up Ansys Maxwell with the above settings on the local lnx4115 machine, benchmarking tests comparing the Maxwell setup to previous Opera magnetostatic simulations were performed. More detailed results can be seen in the Appendix in Tab. 7.2. All good field values differed from Opera values by less than 3%. This slight discrepancy is twofold. Firstly, the non-linear hysteretic residual was taken as 2% to minimise computational time. Secondly, a slightly different technique was employed for field evaluation: Opera reports take the value at the centre of the model, whereas Maxwell models took a mean of a slightly wider 10 mm × 10 mm good field region (GFR) centred on the model centre. When these are taken into account, the models are in good agreement, and the Maxwell setup was deemed adequate. All of the following simulations assume no Eddy current effects. Eddy current density was found to be well below 1% that of coil current density for the frequencies explored, and was judged to be a good approximation for $f < 20$ Hz.

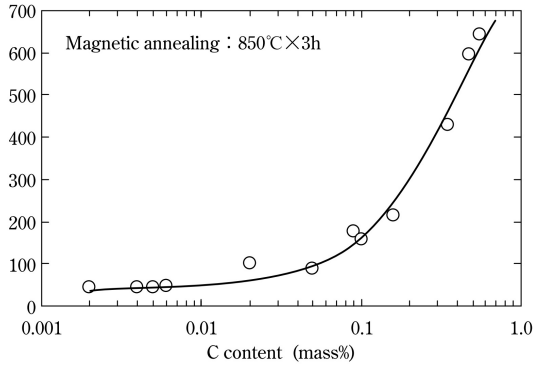

(a) Carbon content dependence of the coercive force, from [3]

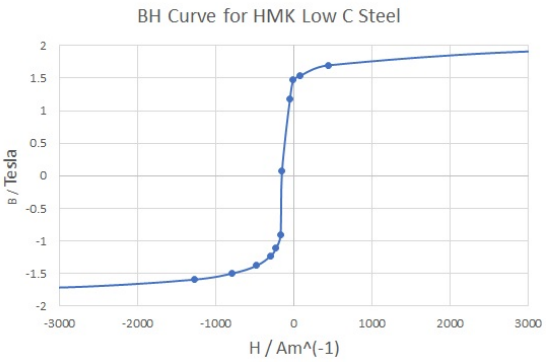

(b) B-H curve used in simulations

Figure 4: Material properties used

3.2 Degaussing Simulation Setup

Degaussing simulations were done in two stages. First, the hysteretic state was prepared by the following waveform:

$$I(t) = \frac{I_0}{1 + e^{2000(t-t_0)}},$$

which corresponds to a constant current of $I_0 = 186.8\,\mathrm{A}$ turned off at $t_0 = 0.5\,\mathrm{s}$. This current value was chosen as it is the highest specification value in [1], and hence contributes most to remnant fields. This process resulted in the hysteretic state with a hysteresis of 13.6 G in the GFR introduced above. This was deemed to adequately represent the real hysteresis for qualitative degaussing study, and formed the initial state for all following degauss simulations. The full yoke hysteretic state can be seen in Fig. 5. Slight asymmetry is the result of finite mesh sizes and non-linear residuals. After setting up the hysteretic state, degaussing was performed with the following current excitation fed into the trim coils:

$$I(t) = \frac{I_d e^{-w(t-t_1)} \cos(2\pi f(t-t_1)}{1 + e^{-2000(t-t_1)}},$$

i.e. a decaying sinusoidal pulse starting at $t_1 = 1\,\mathrm{s}$ with magnitude I_d, frequency f, and decay constant w. An example of the input current waveform can be seen in Fig. 6. The time steps in transient simulations were chosen as small enough to avoid aliasing, but large enough to avoid long computational times. In practice, a suitable time-step was identified as roughly $\Delta t[s] = 0.1 \times \frac{1}{f[Hz]}$, where f is the frequency of a sinusoidal input signal. The errors were taken to be 1.5 G, coming mainly from coarse meshing, non-linear residuals, and insufficient time to reach a steady state.

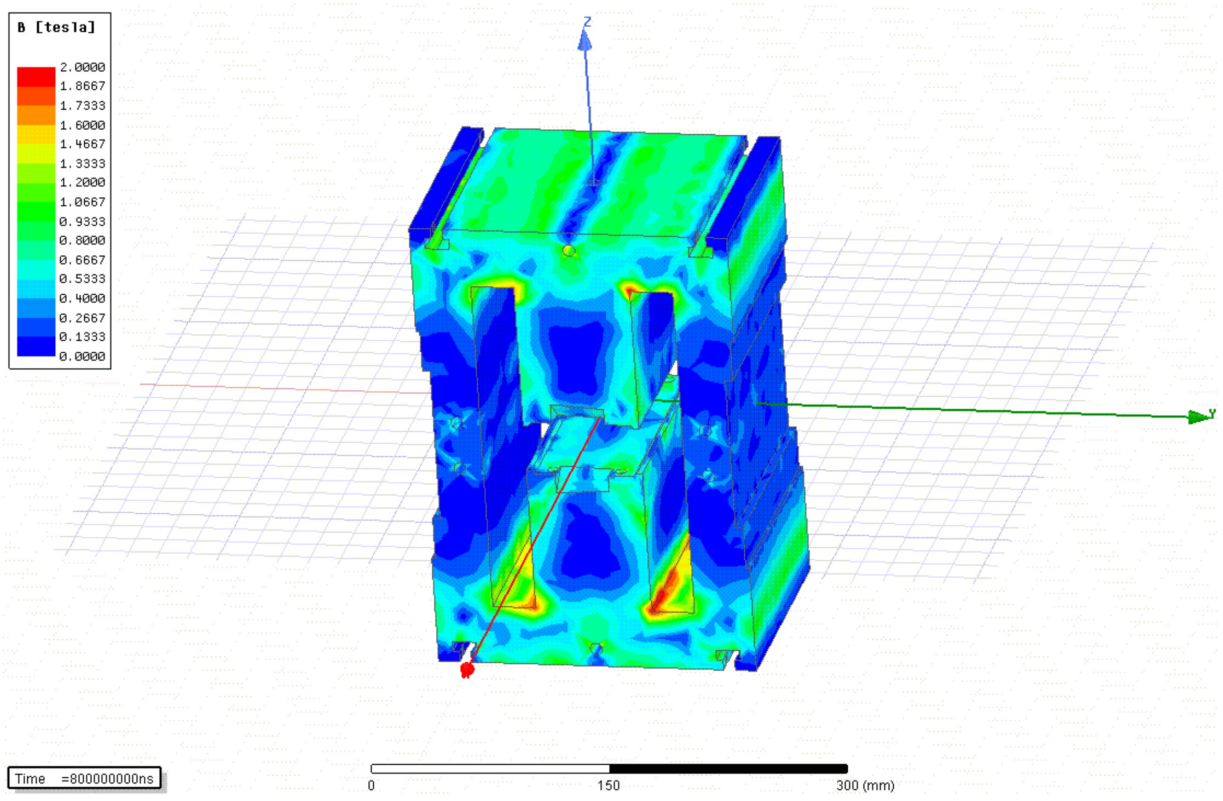

Figure 5: Yoke B field magnitude after turning off $I_0 = 186.8\,\mathrm{A}$

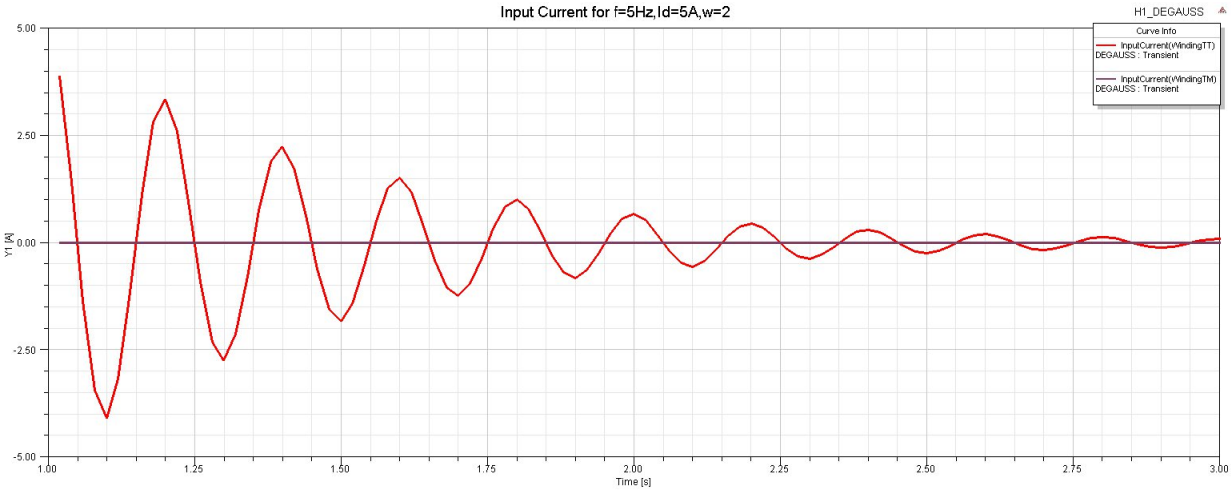

Figure 6: Input Trim Coil Current for $f = 5\,\mathrm{Hz}$,$I_d = 5\,\mathrm{A}$, $w = 2\,\mathrm{s}^{-1}$

3.3 Degaussing Parameter Space Results

Parameter space was scanned to try and identify optimal degaussing parameters.

3.3.1 Amplitude

The first parameter explored was the degaussing pulse amplitude. We need to induce a field large enough to counter the remnant field. From back of the envelope calculations, we expected appreciable degaussing at currents of orders of a few amps, hence the range from 1 A to 100 A was scanned. The particular frequency and decay constant were chosen as $f = 3\,\mathrm{Hz}$ and $w = 0.5\,\mathrm{Hz}$. These were chosen so that the system is subject to a number of oscillations before it decays. Other frequencies and decay constants were also tried, but the qualitative effect of changing the current magnitude remained the same. The results can be seen in Fig. 7. As expected, degaussing is more efficient with higher currents. Degaussing becomes significantly more efficient around $I_d = 6\,\mathrm{A}$, as was predicted by simple theoretical arguments. Field becomes consistent with zero around $I_d = 50\,\mathrm{A}$ within error bounds.

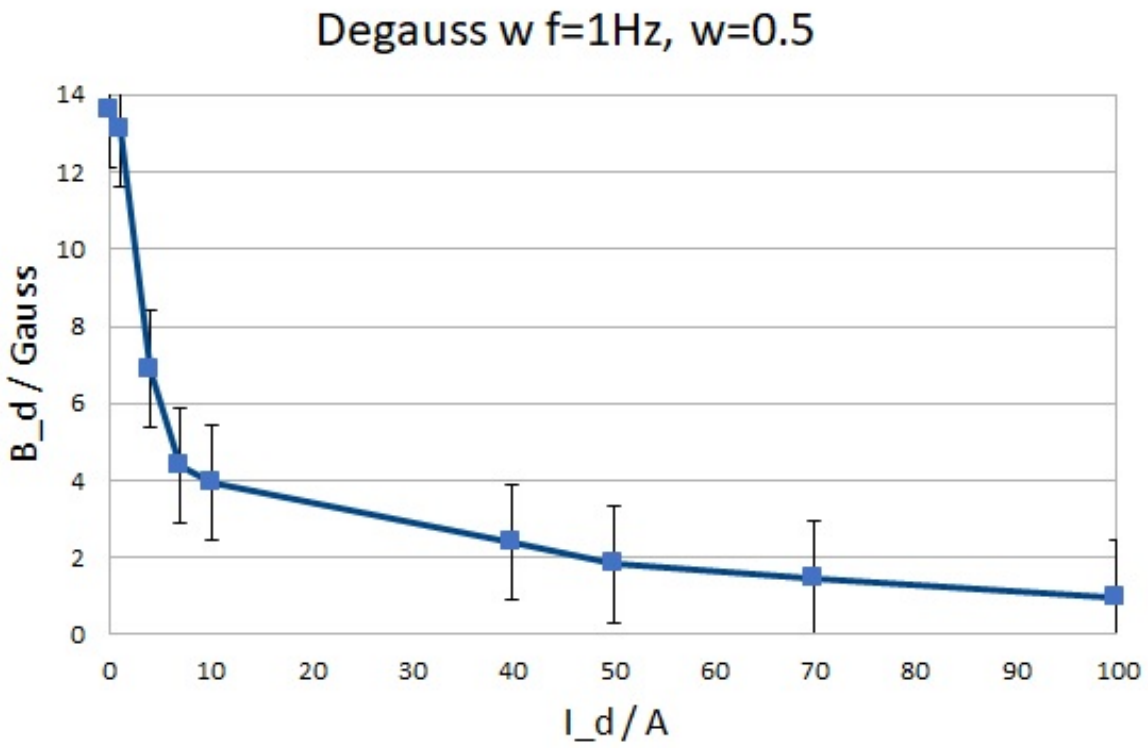

Figure 7: Final field magnitude depending on degaussing current magnitude with $f = 3\,\mathrm{Hz}$ and $w = 0.5\,\mathrm{s}^{-1}$

The magnetic flux density waveforms shown in Fig. 8 confirm that higher magnitude excitation currents lead to a lower magnetic flux density once the steady state is reached.

3.3.2 Frequency

Next varying frequency under a constant current magnitude and decay constant was explored. It was expected and observed that frequency is not the limiting factor in the degaussing procedure so long the frequency is high enough to induce multiple oscillations before the current decays beyond an appreciable value. This can be seen in Fig. 9. Qualitatively, at least three changes

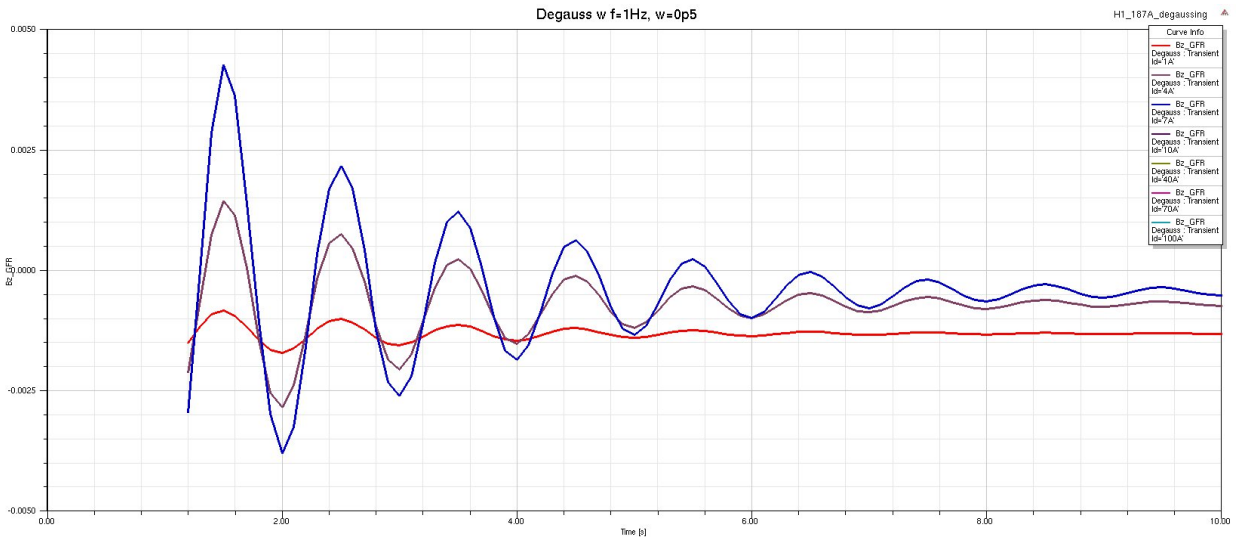

Figure 8: GFR magnetic flux density (/T) over time for $f = 1\,\mathrm{Hz}$ and $w = 0.5\,\mathrm{s}^{-1}$, currents of $I_d = 1\,\mathrm{A}$, 4 A, and 7 A

in field direction were needed to significantly erase the system's memory and have an appreciable degaussing effect. In the limit $f \gg w$, changes in frequency become insignificant.The iron domains would fail to be able to respond to field changes at even higher frequencies, but for our low carbon steel this point is well above any frequencies of interest for degaussing (GHz or above, as observed e.g. by [2]).

3.3.3 Decay Rate Constant

The last important parameter is w, the rate at which the current pulse amplitude decays. This is a related effect to the frequency and hence has a similar explanation. If the pulse decays too quickly, the field is not re-oriented enough times to erase the memory. However, if the decay constant is much smaller than the frequency, we are in the continuum limit of return branches (see Sec. 2.1.1 for more details) and degaussing becomes efficient. This is apparent in Fig. 10, where degaussing only becomes significant when $w \ll f$. An example of what happens if $w > f$ is shown in Fig. 11. The initial degaussing pulse raises the field, but as it never reverses, it only slowly decays to the initial hysteretic state.

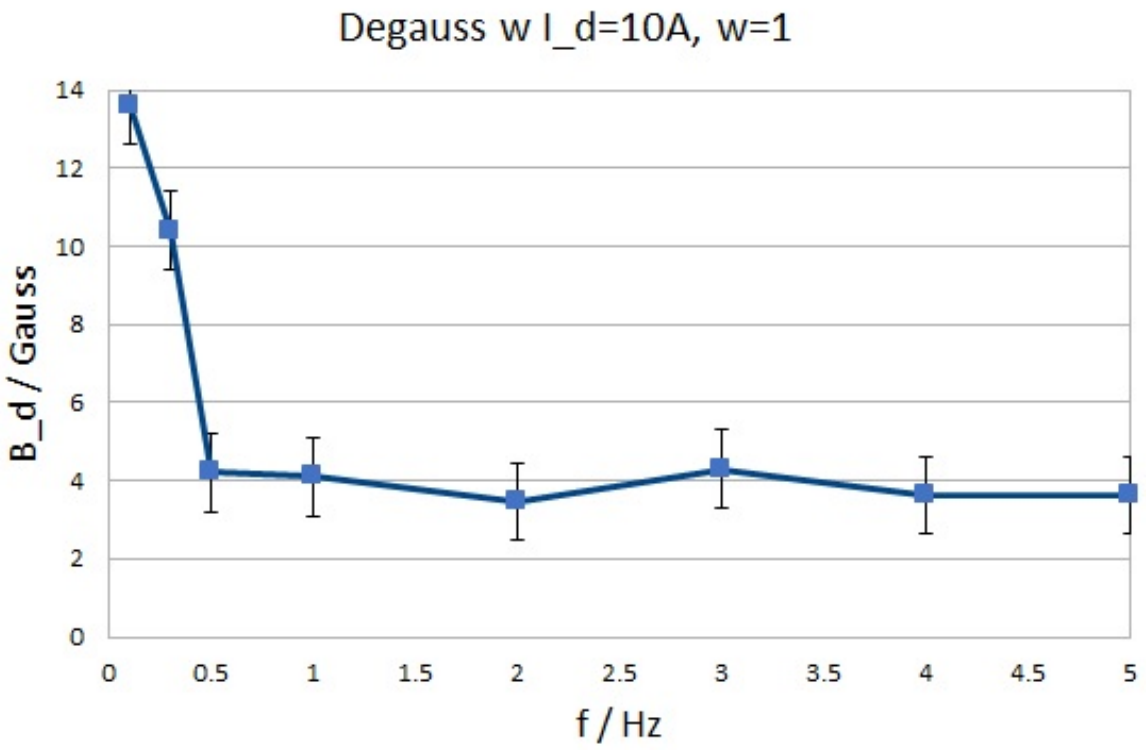

Figure 9: Final field magnitude depending on degaussing frequency with $I_d = 10\,\mathrm{A}$ and $w = 1\,\mathrm{s}^{-1}$

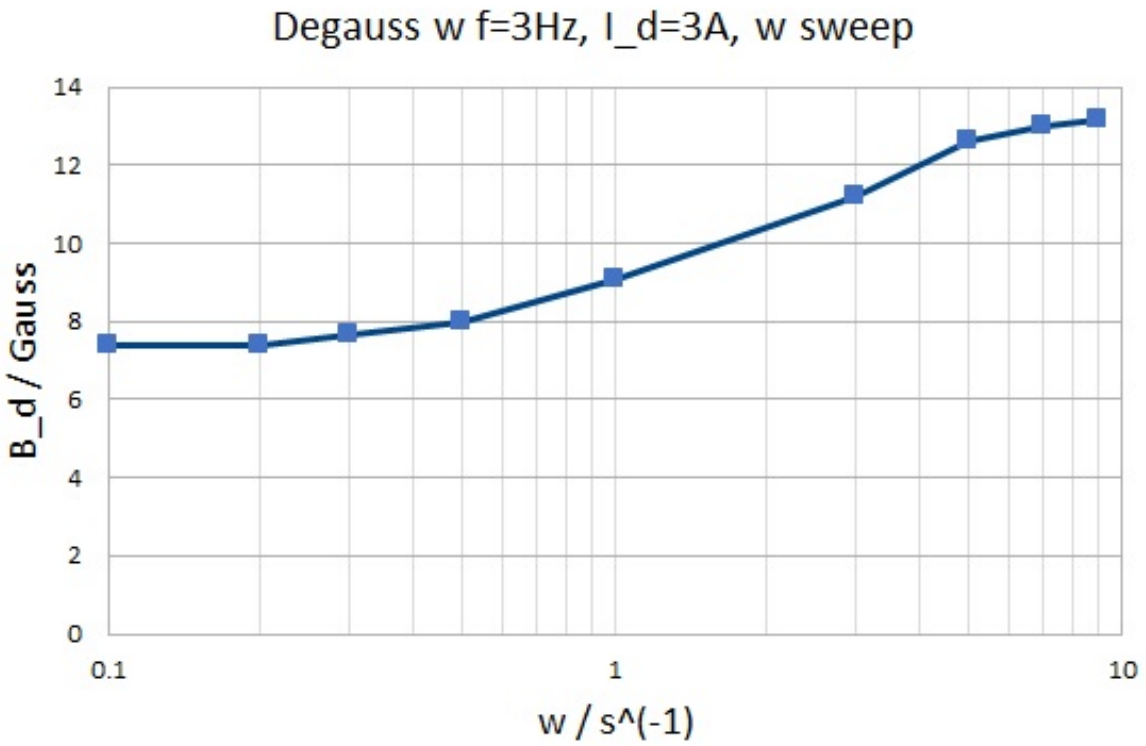

Figure 10: Final field magnitude depending on degaussing decay constant with $I_d = 3\,\mathrm{A}$ and $f = 3\,\mathrm{Hz}$

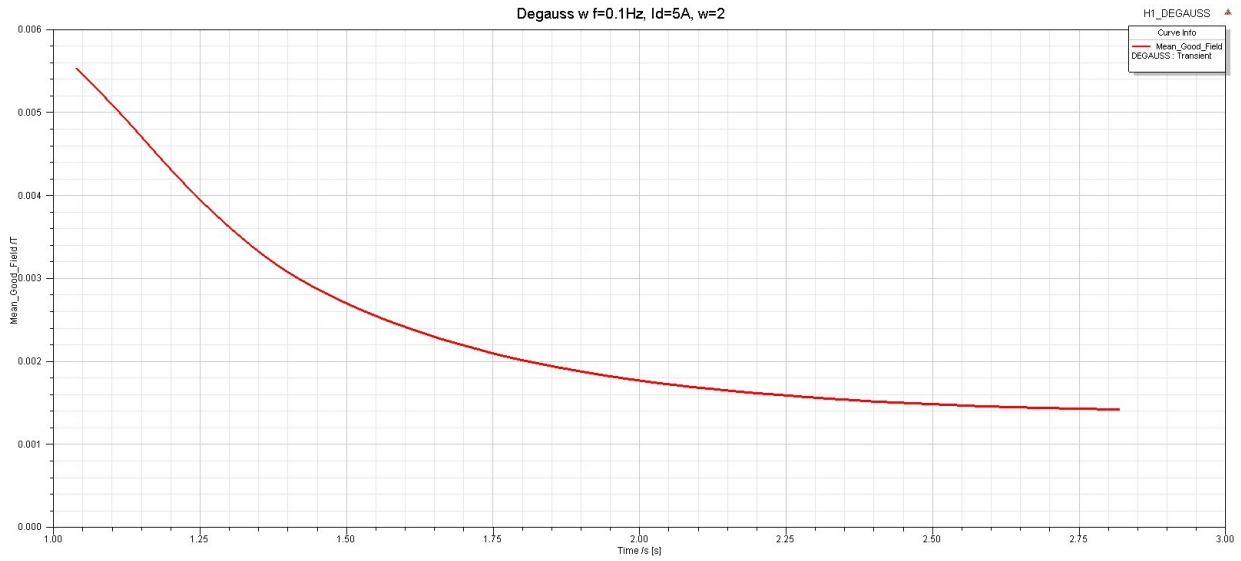

Figure 11: GFR magnetic flux density (in Tesla) versus time for $f = 0.1\,\text{Hz}$, $I_d = 2\,\text{A}$, and $w = 2\,\text{s}^{-1}$.

3.4 H1 as a Circuit Element

Next the same geometry was subject to a sinusoidal voltage excitation on a fixed magnitude in order to find out AC circuit properties of the electromagnetic system. The mesh and material assignments used were identical to those used in the degaussing simulations. In each case, a simulation was run until transients died away and only the steady state solution remained, with a time constant of about $\tau = 1\,\text{s}$.

3.4.1 Real Impedance Results

The yoke is modelled as a linear material of $\mu_r = 4000$ with hysteresis off, and the circuit element behaves as a combination of a resistor of resistance $R = 28.3\,\text{m}\Omega$ and an inductor of inductance $L = 5.7\,\text{mH}$ in series. Thus the complex impedance is simply $Z = R + j\omega L$, as is clear from right parts of Fig. 12 and Fig. 13. These values compare well with estimates outlined in the theoretical section.

When hysteresis is turned on, the resistance becomes more complex. At large frequencies, it grows linearly with frequency. This is because each pass around the hysteresis loop gives a fixed amount of loss (independent of frequency, in a simplistic model), and the number of loops per second is proportional to the frequency. At low frequencies, the resistance is equal to that of the bare coil, i.e. $R = 28.3\,\text{m}\Omega$. This also makes sense, as $R = R_{\text{coil}} + R_{\text{hyst}}$. The transition between these two regimes was found to be complex and voltage-dependent. It depends on the precise details of the evolution of the $B - H$ curve with frequency and voltage (current). This was not pursued due to time constraints of this project.

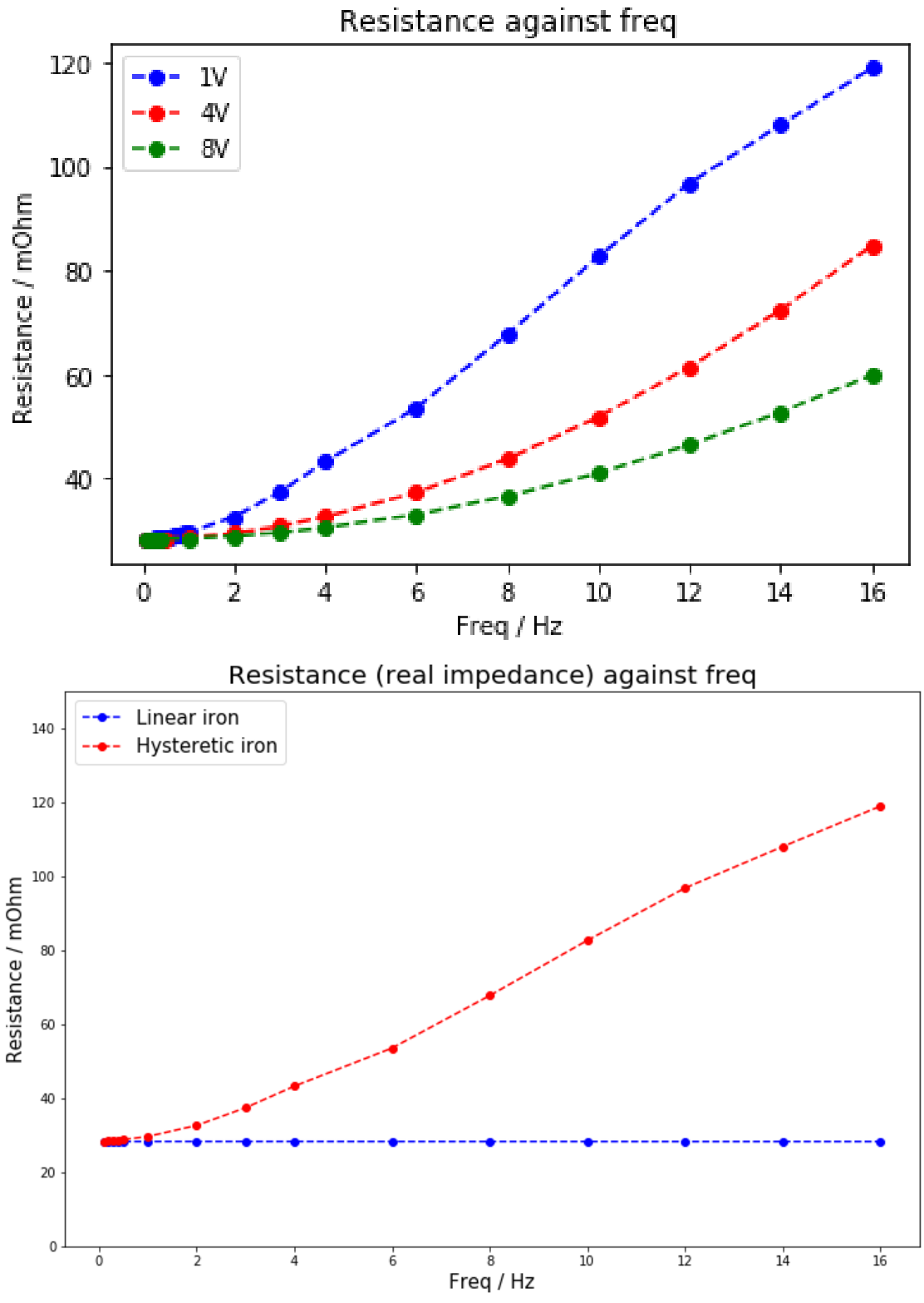

Figure 12: Real Impedance against frequency for multiple voltages (left) and material types (right)

3.4.2 Imaginary Impedance Results

The reluctance for a linear yoke without hysteresis is simply proportional to the frequency. For a hysteretic model, this is true only for low frequencies, as can be seen in Fig. 13. Past the transition explained above, the reluctance begins to saturate, becoming a constant in the large frequency limit. The corner frequency of this transition increases with voltage, i.e. linear behaviour is observed for more frequencies if the voltage is higher. Phenomenologically, it was found this behaviour is consistent with

$$L(\omega) = \frac{L_0}{1 + \frac{\omega}{\omega_c}},$$

with the reluctance then being $\mathcal{R} = \omega L(\omega)$. This situation is complex due to the field inside being non-uniform, and a theoretical explanation for why the inductance falls in this manner was not found. It is expected that the changing $B - H$ curve area is at play once again, as is partial saturation in the yoke.

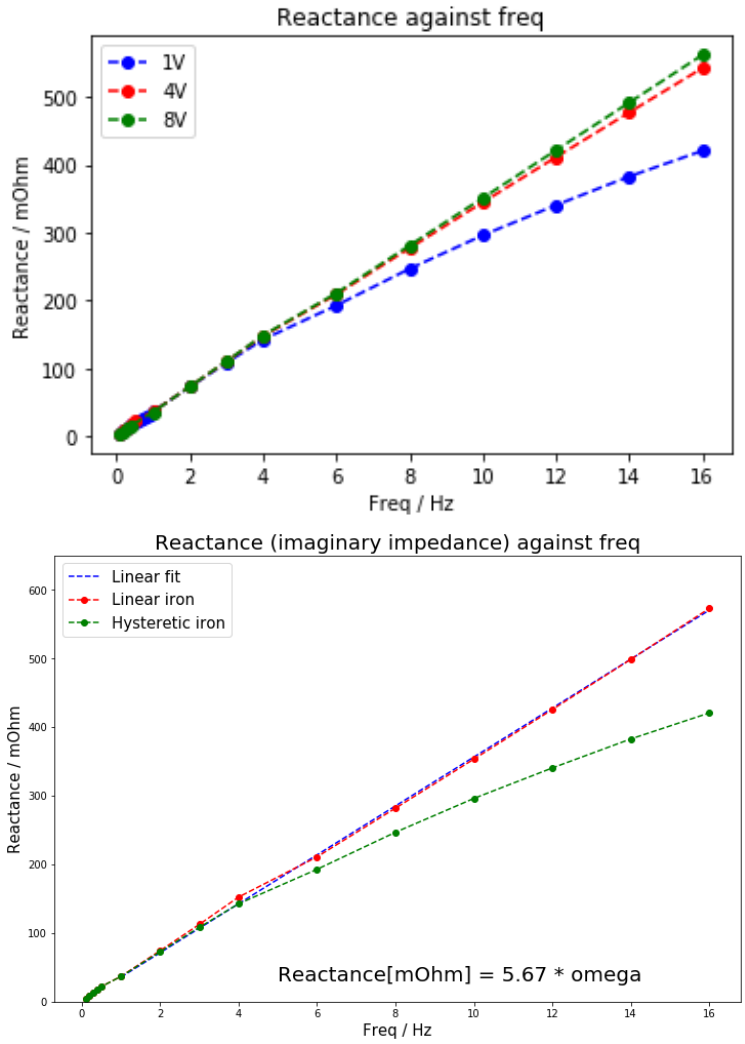

Figure 13: Imaginary Impedance against frequency for multiple voltages (left) and material types (right)

3.5 Numerical Stability of the Simulation

The simulation was unstable for small voltages below 50 mV. It is expected that better stability could be achieved with smaller time-steps, finer meshing, and non-linear residuals. This was not done due to time constraints and no practical interest in such low voltages from CBETA's point of view. The instability development can be seen in Fig. 14. A sinusoidal current solution with a matching frequency to that of the voltage excitation breaks down, and results in step transitions between maximum and minimum current values.

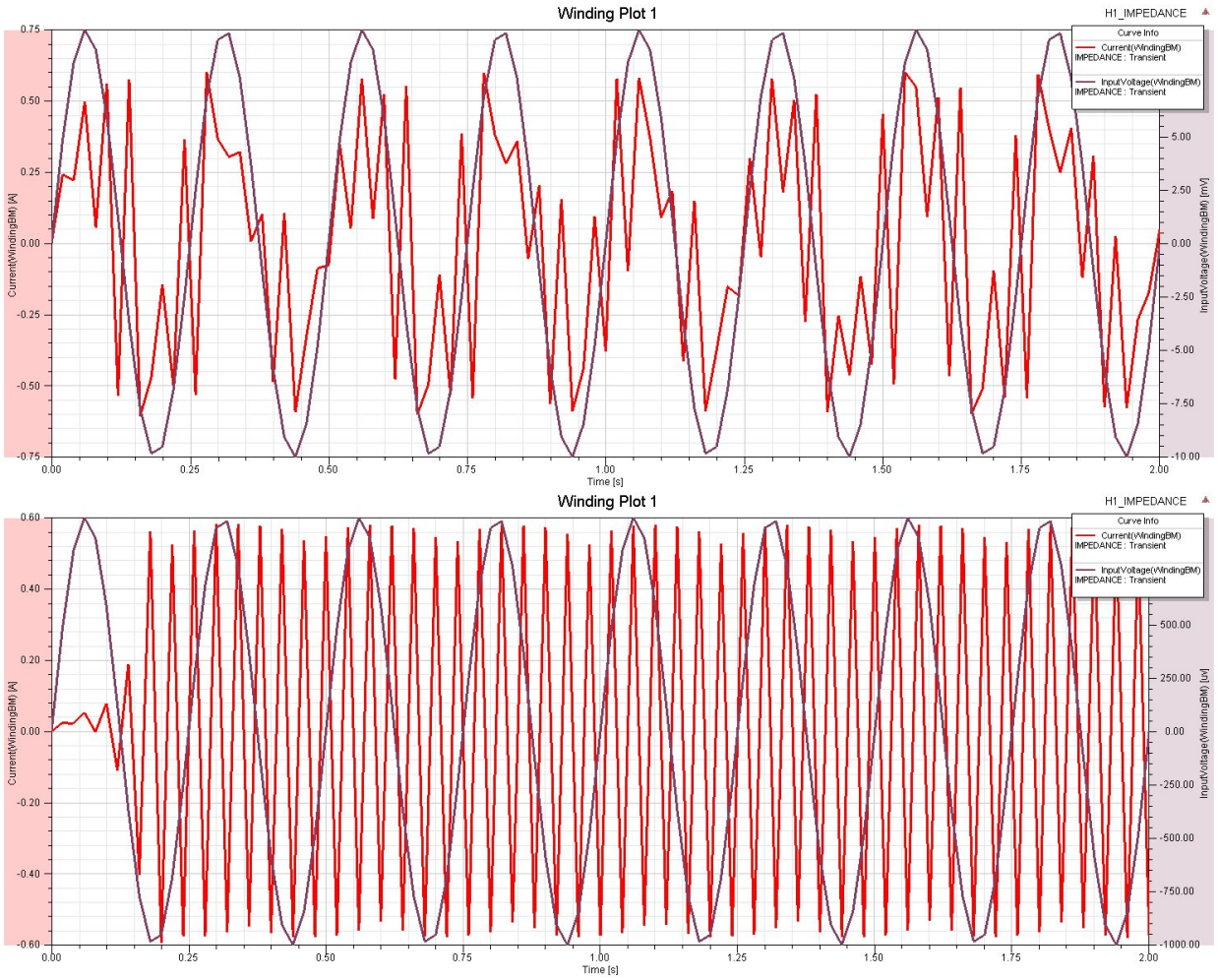

Figure 14: Development of a numerical instability at low voltage excitations: 10 mV (top) and 1 mV (bottom)

4 Experimental Studies of H1

4.1 Experimental Procedures

After computational studies of H1, it was desirable to compare simulation results to real Hall probe measurements. The following procedures were devised and approved by the CBETA Safety Officer for such a purpose. This set of experiments did not require anything beyond what was fully installed on the beamline and available in the room at the time. Specifically, access to the following was

needed:

- RX side H1 short dipole magnet: 11.6V/205.5A max
- Hall effect magnetic field probe
- 3A bipolar power supply: Sigma-Phi 12 channel, bipolar 3A/8V max
- Dual conductor cable, 16 AWG minimum
- Main coil unipolar 187A power supply: TDK-LAMBDA GENH40-250, 40V/250A max or TDK-LAMBDA GENH15-220, 15V/220A max
- EPICS control system for the power supplies
- Non-conductive Kapton tape

In all of the following experiments, we assumed an installed SX side H1 magnet in the beamline with a main coil power supply and corresponding control software. The first step in all cases was to attach a Hall probe to the top of the vacuum pipe with a piece of tape, as centrally as possible. The Hall probe was not moved during the procedures and data recording once in place.

4.1.1 Reproducible Field Production

This procedure explored various strategies to create a reproducible field using only step-like changes in the current exciting the main coil. The procedure was as follows:

Procedure 1 - Max to Operating Value (*MaxOp*)

1. Drive current to maximum as specified in CBETA documentation (187 A), record B field value
2. Lower current to operating value I_0, record B field value
3. Drive current back to maximum, record B field value
4. Lower current back to I_0, record B field value
5. Repeat until a clear asymptotic value is reached

Procedure 2 - Max to Zero (*MaxNull*)

1. Drive current to maximum as specified in CBETA documentation (187 A), record B field value
2. Lower current to zero, record B field value
3. Drive current back to maximum, record B field value
4. Lower current back to zero, record B field value
5. Repeat until a clear asymptotic value is reached
6. Bring current to operating value I_0, record B field value

The above was to be repeated with different operating currents I_0, quantitatively noting the effect of each parameter.

4.1.2 Stability Against Corrections

The procedure was as follows:

1. Drive current to operating value I_0, record B field value
2. Increase current up to $I_0 + \Delta I$, record B field value
3. Lower current back to I_0, record B field value
4. Lower current further to $I_0 - \Delta I$, record B field value
5. Repeat until a clear asymptotic value is reached

The above was to be repeated with different I_0 and ΔI, quantitatively noting the effect of each parameter.

4.1.3 Degaussing

Unfortunately, the EPICS software capabilities available at the time did not allow a fast enough refresh rate to directly test the decaying sinusoids simulated in Maxwell. Thus, the following simplified procedure was used:

1. Attach 3 A bipolar power supply to the corrector coils
2. Drive main coil current to maximum as specified in CBETA documentation (186.8 A)
3. Lower main coil current to zero, record remnant B field value
4. Drive the correction coil with a step-like current, stepping between I_d and $-I_d$, repeated n times, record the endpoint B field
5. Iterate the above over the parameter space available: $I_d \in [1, 3]$A; $n \in [1, 10]$

4.2 Experimental Results

Although the Hall probe was attached to the top of the vacuum pipe, as centrally as possible, it was still a few centimetres from the centre due to probe size limitations. Because of this, the results are not directly comparable to simulation results, as those were taken exactly at the centre. It was found that the remnant field in this location was $B_r = 16.3$ G, the initial state for all subsequent work.

4.2.1 Power Supply Stability

It was observed the GENH 15/220 power supply on MS1DIP05 showed strange unstable behaviour above operating currents of 140 A. The Hall probe measured B field would oscillate between two values, with the uncertainty defined as the range of this oscillation. This behaviour, quantitatively shown in Fig. 15, was not observed on the MS1DIP03 with the GENH 40/250 power supply. At the time, no other GENH 15/220 power supplies were connected, and hence it has not been established whether this unstable behaviour is due to a single faulty power supply, a general problem with GENH 15/220, or something else (e.g. MS1DIP05 not being tightened enough, leading to physical oscillations due to magnetic forces, and hence to observed field fluctuations). The full dataset collected is available in Sec. 7.1 in the Appendix.

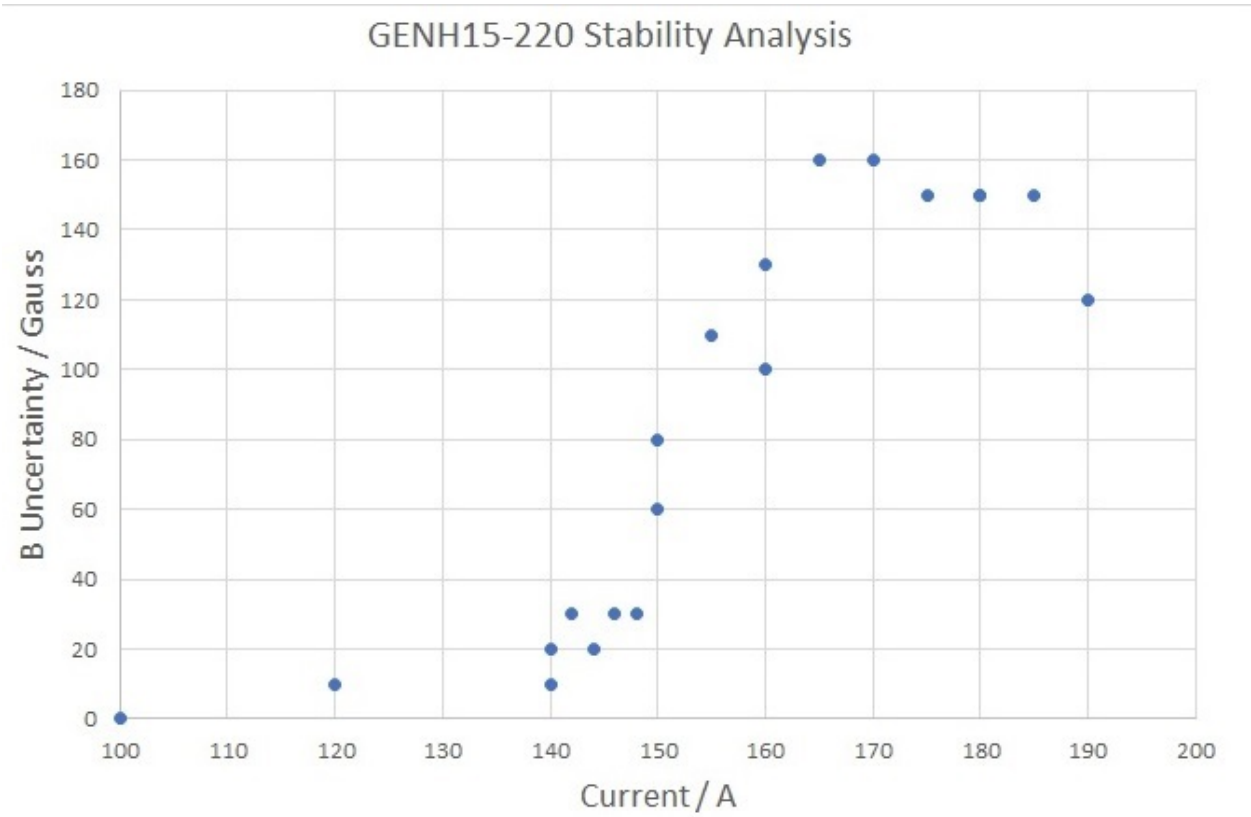

Figure 15: Observed Hall probe field uncertainty against operating current on the MS1DIP05 with a GENH 15/220 power supply

4.2.2 Reproducible Field Production

It is desirable to have a way of always coming back to the same field value regardless of previous hysteretic memory. Two prcedures were designed and tested for this purpose. Example results are given in Fig. 16. Both MaxOp and MaxNull perform well and fulfil the criteria of simplicity and repeatability. They however lead to different operating values, so one needs to be chosen for convenience. As outlined in the procedures above, MaxOp is taking max current - operating current multiple times, wheras MaxNull is taking max current - zero multiple times before going the the operating value. It was found that both lead to a repeatable value, regardless of the starting hysteresis, if they are performed at least 3 times, preferably 5 times.

4.2.3 Stability Against Corrections

During operation of CBETA, small position corrections are often necessary, and are achieved with small current changes. However, after such a change, coming back to the nominal current I_0 does not result in the same field value due to hysteresis. The final field one returns to was measured with the procedure outlined above. Results can be seen in Fig. 17. An operating current of $I_0 = 5\,\mathrm{A}$ was chosen, as this means the field is still below 200 G, which was the lowest and most accurate range on the Hall probe meter. At this range, the uncertainty is only 0.2 G. At higher currents, small changes of a few Gauss were impossible to observe.

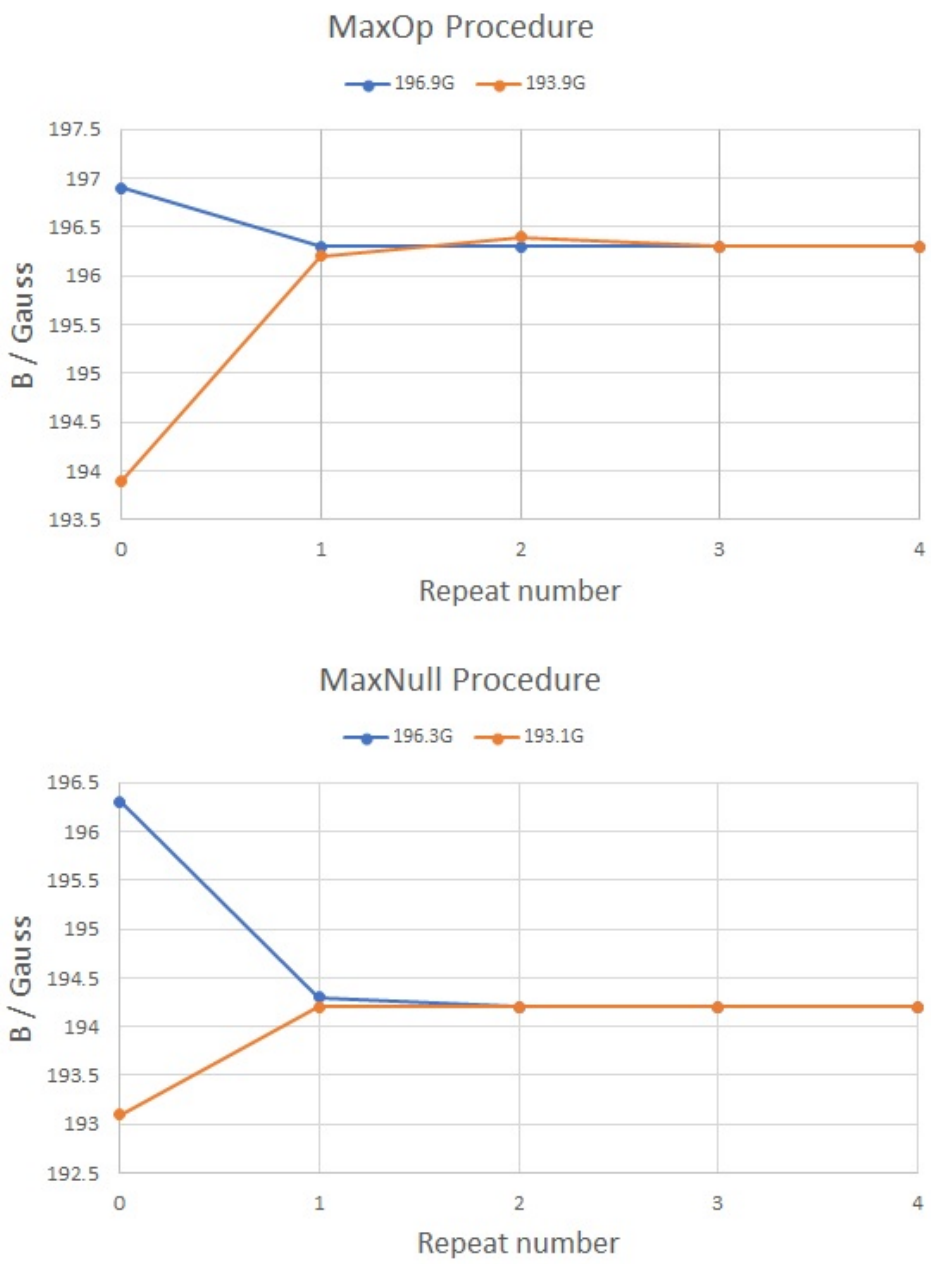

Figure 16: Two reproducible field procedures: MaxOp (left) and MaxNull (right), each repeated from different starting points

Qualitatively, the resultant shape compares well to the same process simulated with Ansys Maxwell. Changes of up to 5 G can be induced just by small current corrections. The figures are not symmetric, because the left side is near zero, where other hysteretic effects come into play. The negative simulated values are simply due to opposite orientation of the Hall probe.

However, actual values do not compare well. This discrepancy was identified as due to a limitation on the quality of the B-H curve used during simulations. The manufacturer admitted that B-H curves vary significantly between magnets, with H_c varying from $20\,\mathrm{Am}^{-1}$ to $160\,\mathrm{Am}^{-1}$ (see [4]).

As this is one of the key parameters for hysteresis, it is difficult to obtain accurate quantitative simulations without knowing the exact value of H_c.

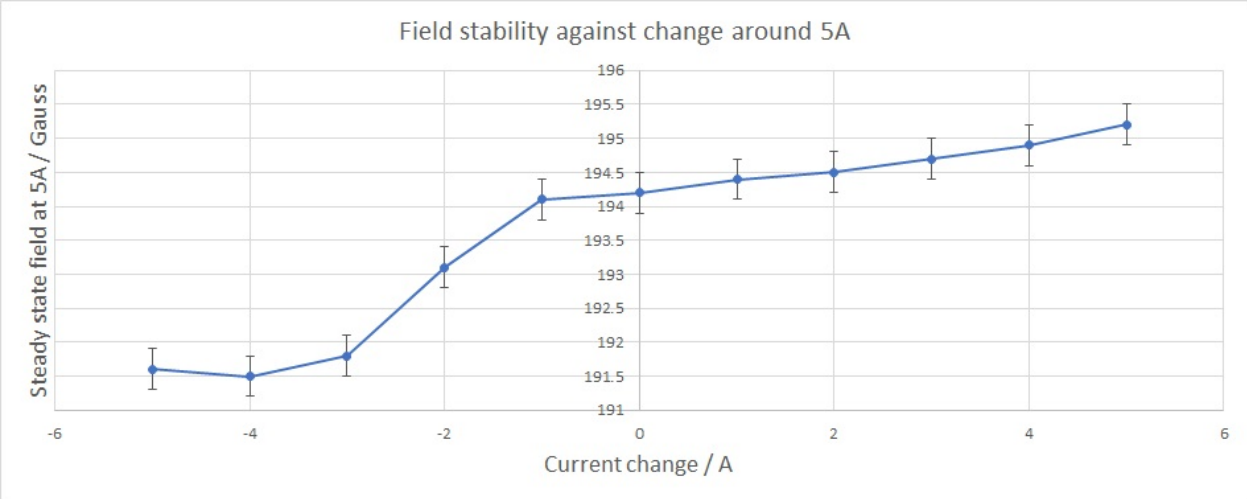

Figure 17: Asymptotic B field value at an operating current of $I_0 = 5\,\mathrm{A}$ after corrections of varying current magnitude ΔI, experimental results

4.2.4 Degaussing

Step-like degaussing was performed with variable amplitude, as outlined in the procedures above. The results can be seen in Fig. 18. As expected from simulations, only partial degaussing was achieved, with $I_d = 3\,\mathrm{A}$ achieving a degaussing of just under 15% (2.1 G) compared to the original 16.3 G. This is somewhat lower than results from simulations, which suggest $20\% - 30\%$ degaussing depending on the decay constant and frequency. Again, this is mainly from a limitation on the quality of the B-H curve used during simulations. More accurate H_c values would be needed to obtain accurate numerical results. Qualitatively, however, the results below support simulation results. Higher currents achieve larger partial degaussing, in an almost linear fashion at the current magnitudes tested. More repetitions result in higher degaussing, with saturation reached after about 5 cycles.

5 Suggested Future Work

Several avenues of research could be pursued, given more time. In descending order of importance:

1. Test the other GENH 15/220 power supplies to see if the stability problems are due to the power supply type, or something else.
2. Choose a procedure for reproducible field production (e.g. MaxOp or MaxNull), and tabulate accurate field values one obtains for each current using this procedure.
3. Alternatively, develop a ringing circuit which can produce the waveforms simulated in above sections to remove the remnant field completely.
4. Undertake current excitation simulations in the same vein as the voltage ones above. Use B-H curve areas obtained from these simulations to explain the transition hysteretic behaviour of

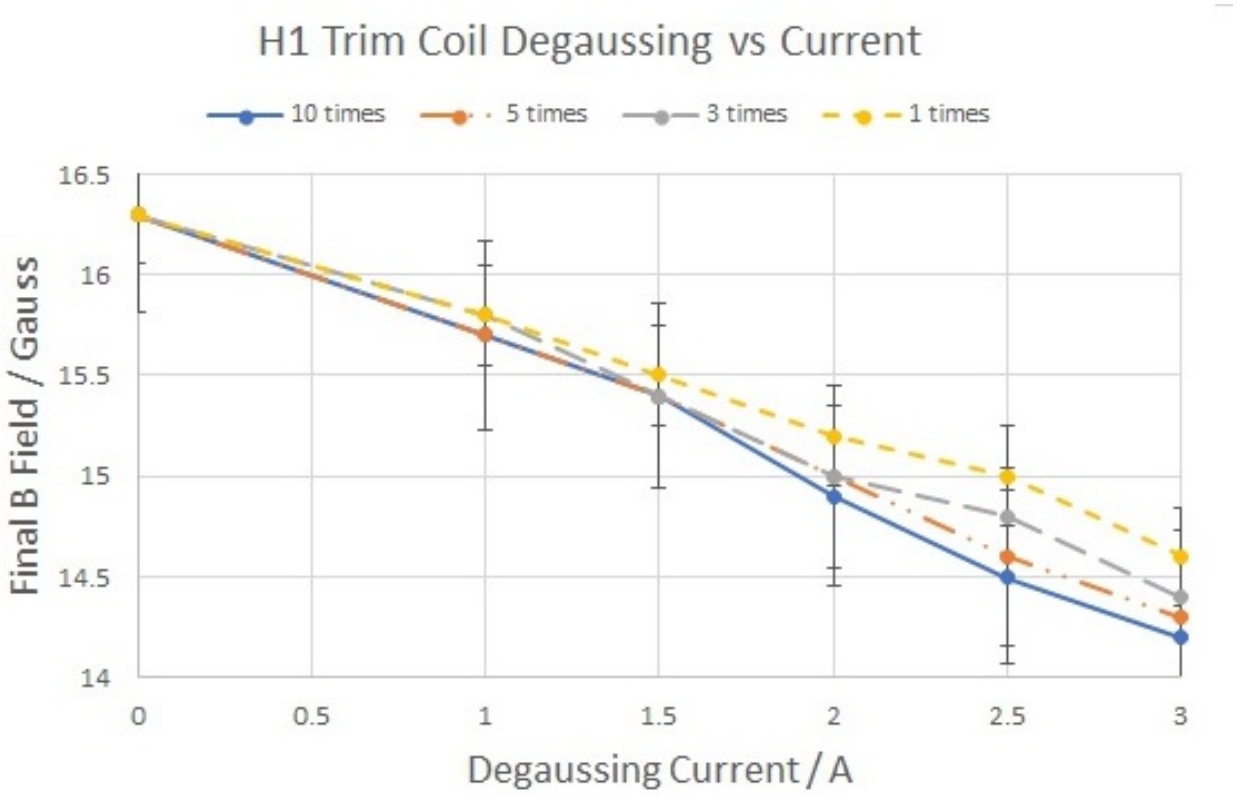

Figure 18: Remnant B field after degaussing with steps performed n times against current magnitude

H1 as a circuit element. Include Eddy current effects if higher accuracy or frequencies are desired.

5. Experimentally measure the B-H curve for the magnets simulated for accurate quantitative result comparisons.

6 Conclusion

In this summer research project, magnetic hysteresis of the H1 CBETA dipole magnets was explored. The goal was to begin the effort towards field reproducibility and mitigating hysteretic effects, as well as theoretically understanding the magnet as a circuit element. The AnsysEM suite with Maxwell 19.2 was used for the hysteretic simulations. The parameter space for a degaussing procedure using the trim coils was explored. It was found that significant degaussing can be obtained with a decaying ringing waveforms of magnitudes above 10 A, so long as the frequency f and decay constant w were chosen such that $f \gg w$.

The circuit properties of the magnet were simulated and explored using a sinusoidal voltage input. It was found that for low frequencies $f \ll 1\,\text{Hz}$, the magnet behaves as a series LR circuit with $R = (28.3 \pm 0.5)\,\text{m}\Omega$ and $L = (5.7 \pm 0.1)\,\text{mH}$. At higher frequencies, hysteretic effects become significant, and resistance becomes proportional to the frequency due to hysteretic losses. Preliminary results with current simulations showed similar behaviour. A drop and saturation in inductance

for higher frequencies was observed in the simulation data. Numerical instabilities were found for excitations with small voltages $V < 50\,\mathrm{mV}$.

Experimental results on degaussing and current corrections were collected with Hall probe measurements on the MS1DIP05. Its monopolar power supply behaved strangely at currents above 140 A, with the field oscillating by as much as 150 G. Partial degaussing was achieved with a 3 A bipolar power supply attached to the corrector coils. Good qualitative agreement with simulation results was found, but due to B-H curve details, mainly the coercivity, quantitative comparisons were inaccurate. Small current changes around a 5 A current set point were found to change the operating field by several gauss. Two procedures, MaxOp and MaxNull, were designed to produce repeatable operating field values to within 0.1 G. MaxOp entails going from the desired current up to highest current specified five times. MaxNull means taking the current between zero and maximum current five times before setting the desired current value. Both were found to have similar efficiency at producing a stable B field value.

More work is desirable to have a robust reproducible field procedure.

References

[1] CBETA magnet tables, known as

`splitter_magnets_4pass_20190520_table V3.xlsx`

David Burke and Jim Crittenden, CBETA Documentation

[2] Degaussing PMR Writer Poles: A Micromagnetic Modeling Study. *Bai et. al.,* IEEE Transactions on Magnetics, Vol. 47, No. 10, October 2011

[3] Development Trends of Soft Magnetic Iron. *M. Chiba,* Wire Rod & Bar Products Development Department, R & D Lab, Iron & Steel Business, Japan, 2011

[4] Manufacturing File for the Cornell CBETA magnets. Elytt Energy, 2017

[5] User's guide, Ansys Maxwell 3D 19.2. ANSYS Inc, 2018

[6] Advanced Hysteresis Modelling Recorded Workshop. *M. Rosu,* ANSYS Inc, 2013

[7] Hysteresis in Magnetism: For Physicists, Materials Scientists, and Engineers, Section 1.2 *G. Bertotti,* Academic Press, 1998

7 Appendix

7.1 GENH 15/220 Stability Analysis Data

Current /A	B_{min} /kG	B_{max} /kG	Uncertainty /G
100.03	3.61	3.61	0
120.04	4.32	4.33	10
140.03	5.01	5.02	10
140.04	5.00	5.02	20
142.03	5.06	5.09	30
144.03	5.13	5.15	20
146.02	5.19	5.22	30
148.08	5.25	5.28	30
150.02	5.29	5.35	60
150.03	5.30	5.38	80
155.02	5.44	5.55	110
160.02	5.59	5.69	100
160.02	5.57	5.70	130
165.02	5.70	5.86	160
170.02	5.84	6.00	160
175.02	5.98	6.13	150
180.02	6.10	6.25	150
180.02	6.10	6.25	150
185.01	6.23	6.38	150
190.03	6.36	6.48	120
200.02	6.57	6.70	130

7.2 Opera Benchmarking Results

I / A	B Maxwell / T	B Opera / T	% diff
186.8	0.6348	0.6519	2.62
180.7	0.6140	0.6306	2.63
179.0	0.6082	0.6245	2.60
140.2	0.4762	0.4891	2.64
122.4	0.4157	0.4270	2.64
74.4	0.2528	0.2598	2.69

7.3 Maxwell Mesh Statistics

	Num Tets	Min edge length /mm	Max edge length /mm	RMS edge length /mm
Coil_bot_1	1074	11.78	54.08	34.63
TrimCoil_bot_1	285	9.53	46.43	28.79
Coil_top_1	1130	10.79	60.03	34.71
TrimCoil_top_1	300	9.53	48.15	27.79
Yoke	17552	0.73	35.69	22.84
Region	20149	0.93	50.74	27.81